JOURNAL OF MATERIALS SCIENCE: MATERIALS IN MEDICINE **16** (2005) 183–188

Measurement of mechanical properties of rectal wall

Y. QIAO[1,*], E. PAN[1], S. S. CHAKRAVARTHULA[1], F. HAN[1],
J. LIANG[2], S. GUDLAVALLETI[3]
[1]*Department of Civil Engineering, University of Akron, Akron, OH 44325-3905, USA*
E-mail: yqiao@uakron.edu
[2]*Department of Radiation Oncology, William Beaumont Hospital, Royal Oak, MI 48073, USA*
[3]*EPT Lifing Technologies, GE Global Research Center, Niskayuna, NY 12309, USA*

In this paper, a pig's rectum was studied as a model biomaterial and its mechanical behaviors under tensile, compressive, and shear stresses were measured accurately using a multipurpose microtesting system. Based on the stress-strain relations of samples of different orientations, the tangential moduli were calculated through a reverse method combined with self-correlation analysis. The experimental data exhibited pronounced nonlinear and anisotropic characteristics. It was found that the effective compliance in tension along the longitudinal direction was larger than that along the circumferential direction, but smaller than that along the out-of-plane direction.

1. Introduction

The accurate measurement of mechanical properties of soft tissues are of basic scientific interest and immense technological importance to a variety of clinical practices such as organ registration [1, 2], dose optimization [3], tumor detection [4, 5], hyperthermia treatment [6], and so on, and has been an active research area for decades. On the one hand, the external loads applied on the samples, which are often of the dimensions around several millimeters, are usually less than 1–2 N, which demands a high accuracy of load transducer around 10^{-2} N (0.5% of the full scale) and the fine resolution of displacement sensor in the range of 5–50 μm [7]. On the other hand, the large extent of deformation up to 150% makes the application of most of conventional low-level-signal transducers, e.g. piezoelectric loadcells, irrelevant. Furthermore, in tissue dynamics studies, very often pre-conditioning is required to minimize the degree of history dependence so as to assure that the experimental data can reflect the *in-vivo* organ behaviors [8]. Because of these difficulties, currently the reliable experimental results of soft tissues, e.g. rectal walls, are rare [9]. The limited literature data are either based on simple methods that can only provide order-of-magnitude assessments [10–14] or cannot reflect the nonlinear/anisotropic nature of the biomaterials [15–18].

One way to solve these problems is to use small-scale, high-compliance testing frames, which can be broadly classified into two groups: integrated systems [19–21] and non-integrated systems [22, 23]. In the experimental studies on individual cells, the former, for which the sample and the testing machine must be placed on the same wafer, are more widely applied. However, for soft tissues, the complexity in sample preparation and assembly can be prohibitively difficult.

Recently, based on a research on microtesting technologies [24], a multipurpose non-integrated microtesting system has been built up in one of the authors' lab. A two-compound-flexure structure was employed to assure the precision positioning. The displacement resolution is 20 nm, which is close to the molecular level; and the load resolution is at the level of tens of μN. The accurate and repeatable performance of the system has been documented in [24]. By using different holding stages this system can be applied to perform microscale tensile, compression, bending, shear, and nano-indentation tests.

2. Experimental

The pig's rectum samples studied in this paper were provided by the Strasburg Provision, Inc. Immediate after being separated from the animal body, the fresh rectum was cut open along the longitudinal direction, cleaned with cold water, and stored in water at room temperature for less than 0.5 h before testing. The effect of osmotic swelling will be ignored in the following discussion. The average thickness of the rectal wall was measured to be 1.7 mm through the high-resolution digitalized images of the sample profile taken by a Nikon CP4500 camera.

---

*Author to whom all correspondence should be addressed.

0957–4530 © *2005 Springer Science + Business Media, Inc.*

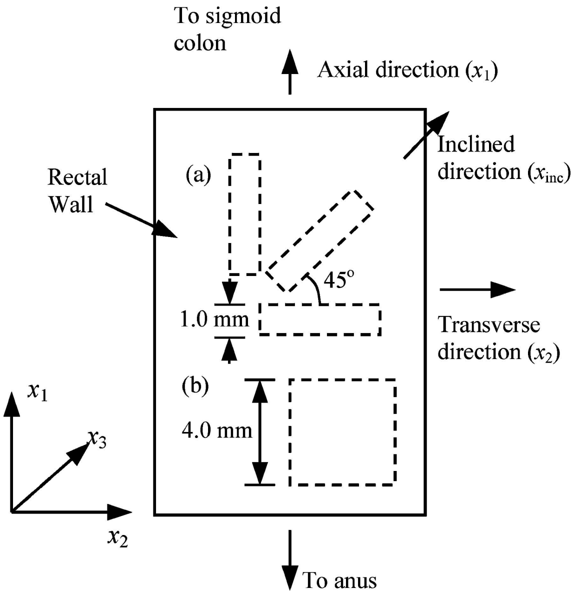

Figure 1 (a) Tensile specimens and (b) shear/compression specimens of the rectal wall.

By using a parallel blade couple, tensile specimens were cut along three different orientations from the rectal wall on a flat cutting stage: x_1, x_2, and x_{inc}, as depicted inFig. 1. Direction x_1 is along the longitudinal axis; x_2 is along the circumferential (transverse) axis, and x_{inc} is 45 ° away from them. The uncertainty in tissue orientation mostly came from the misalignment of the parallel blades and the guiding marks in the cutting stage, which is at the level of ± 0.5 °. The areas of large horizontal folds and anal columns were avoided. The specimen width was 1.0 mm. The specimens for shear and compression tests were cut through the similar procedure with the in-plane dimension of 4.0 × 4.0 mm and the edges parallel to x_1 and x_2, respectively.

Fig. 2(a) depicts the tensile experimental set up. Type 18-8 locking washers were applied such that the grips could be self-tightened even when the relaxation of the rectal wall was significant. The specimen was first fixed between the loading plates and the holding plates at the working station, and then mounted on the microtesting machine through a self-aligning and self-locking track. To avoid sample slippage in the grips, a superglue was applied between the sample and the holding plates. The holders and alignment devices, as well as the body of the compound flexure frame, were made from A17075 aluminum alloy. One of the loading plates, "A", was connected to the displacement compound flexure, and the other, "B", was attached to the loadcell compound flexure. Initially the distance between plates "A" and "B" $l_0 = 1.0$ mm. Through the displacement controlled precision actuator attached to the displacement compound flexure, plate "A" was driven with a constant rate of 0.1 mm/sec. Due to the specimen stiffness, plate "B" moved with "A", causing the displacement of loadcell compound flexure. With the frame compliance that has been calibrated to be $K = 1.2174$ N/mm, the axial load, P, can be obtained as

$$P = K \cdot \delta_{\mathrm{B}} \tag{1}$$

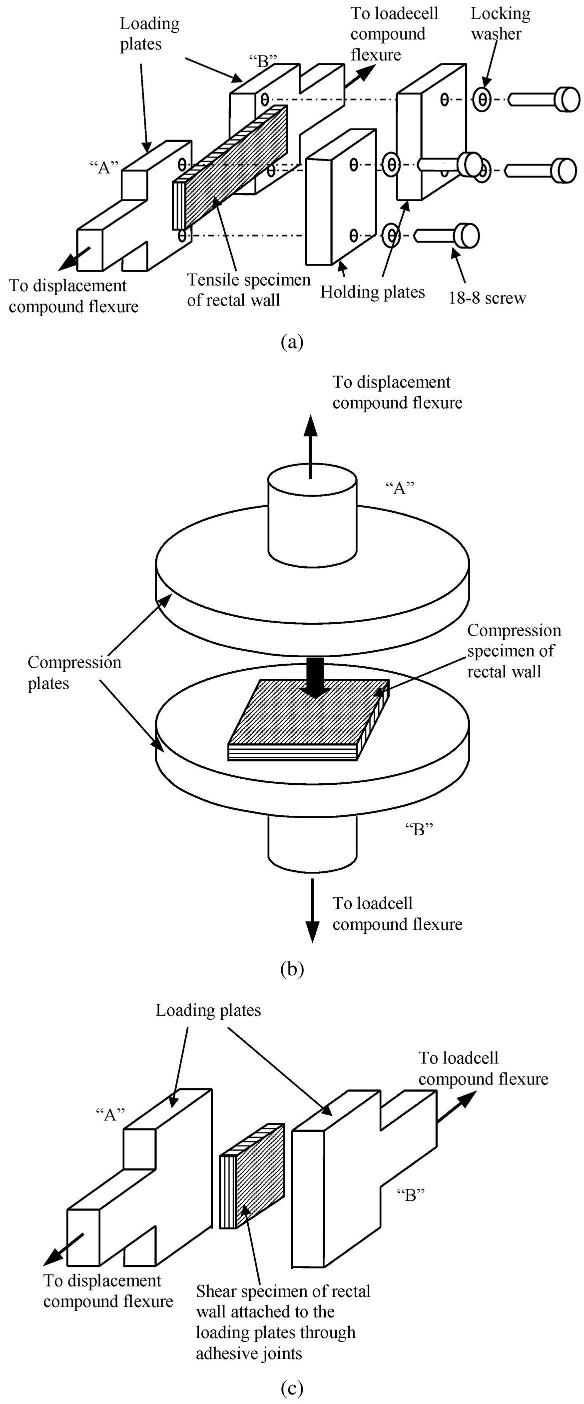

Figure 2 Schematic diagrams of loading stages for (a) tensile test; (b) compression test; and (c) shear test.

where δ_{B} is the displacement of loadcell compound flexure measured through the loadcell sensor. The difference between δ_{A} and δ_{B} gives the elongation of the specimen

$$\delta = \delta_{\mathrm{A}} - \delta_{\mathrm{B}} \tag{2}$$

where δ_{A} is the displacement of plate "A". Thus, the engineering stress and strain can be calculated as P/A_0 and δ/l_0, respectively, with A_0 being the initial cross-sectional area of the specimen. Altogether 10 tensile tests were performed on specimens of different orientations depicted in Fig. 1(a), and the typical stress-strain curves are shown in Fig. 3. Prior to the testing of each sample, four to five pre-fatigue cycles were applied

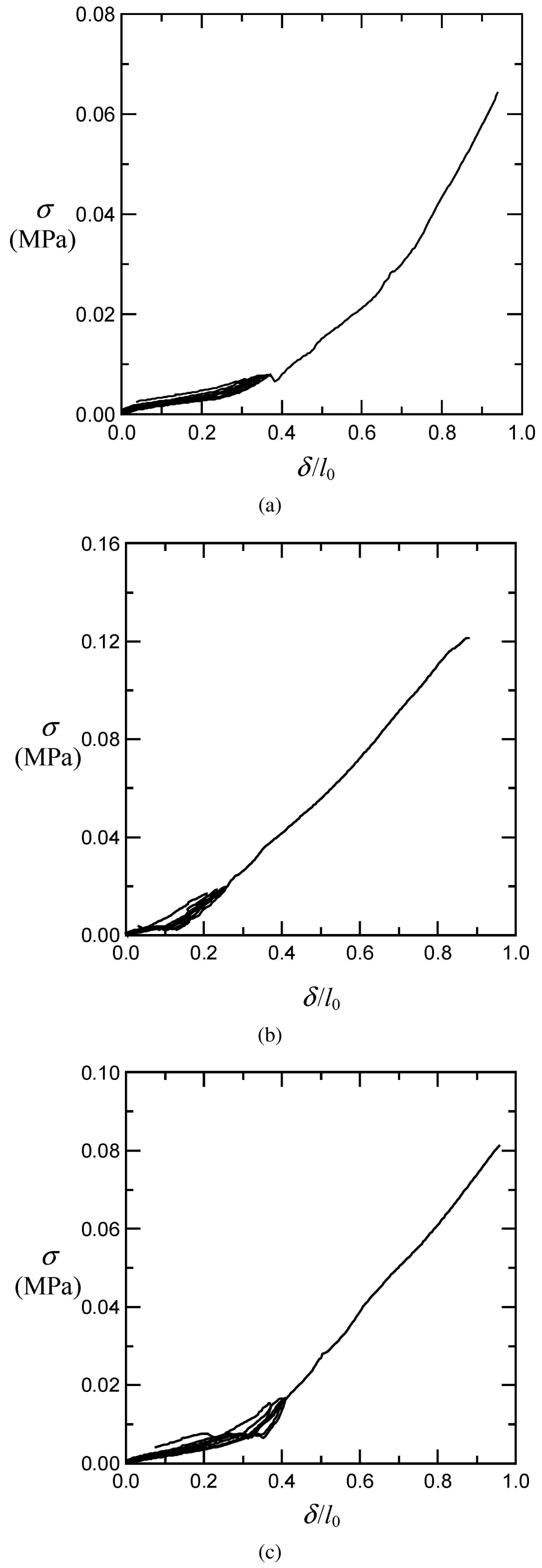

(a)

(b)

(c)

Figure 3 Typical stress-strain curves of tensile tests: (a) along the longitudinal direction (x_1); (b) along the transverse direction (x_2); and (c) along the inclined direction (x_{inc}).

until the hysteresis loops converged, assuring that the degree of history dependence of the material behavior was minimized. The strain range of preconditioning treatment was kept below 0.4 to avoid any possible permanent damages. During the experiment on specimens cut along the x_1 direction, a series of high-resolution photos were taken using a Nikon CP4500 camera for the calculation of the effective in-plane shear resistance, which will be discussed shortly.

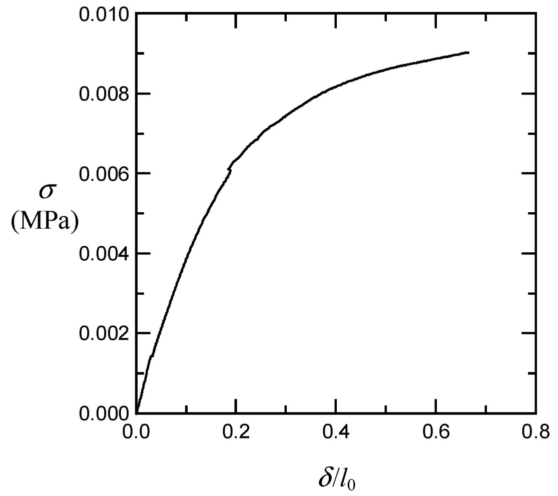

Figure 4 A typical stress-strain curve of compression test along the out-of-plane direction (x_3).

In order to evaluate the out-of-plane compliance, compression tests were performed using two compression plates attached to the displacement and loadcell compound flexures, respectively, as shown in Fig. 2(b). Through Equations (1) and (2) the compressive load and deformation can be obtained by measuring the displacements of the two compound flexures. Altogether three specimens were tested, and a typical stress-strain curve is shown in Fig. 4.

The effective out-of-plane shear resistances were measured through the simple shear tests depicted in Fig. 2(c). The two loading plates were parallel to each other. The distance between them was set to 1.7 mm, the same as the thickness of the rectal wall. The two surfaces of the square shear specimen were attached to loading plates “A” and “B” through adhesive joints, respectively. The shear displacement was taken as $\delta_A - \delta_B$ and thus the effective shear strain could be obtained as

$$\gamma = (\delta_A - \delta_B)/d_0 \qquad (3)$$

where $d_0 = 1.7$ mm is the sample thickness. The effective shear stress, τ, was obtained through Equation (1). A typical shear stress-strain curve is shown in Fig. 5.

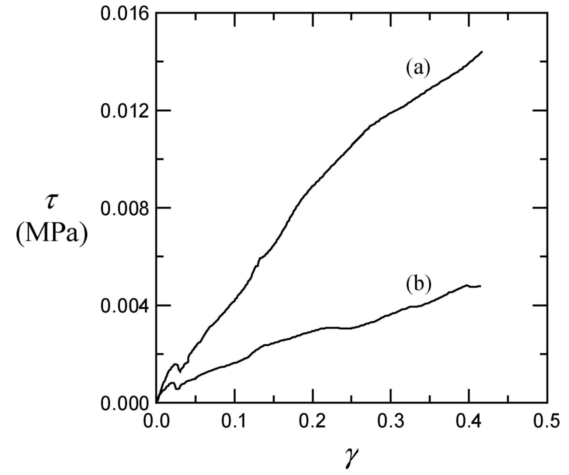

Figure 5 Typical stress-strain curves of simple shear tests: (a) G_{13} and (b) G_{23}.

3. Results and discussion

The stress-strain curves of the rectal wall in Figs. 3–5 exhibit clearly the nonlinear characteristics. In general, therefore, a constitutive model capable of describing these material behaviors is required [8]. In certain biomedical applications, e.g. in image registration and computational anatomy [1, 2], however, it was found that a linear representation is sufficient as a first-order approximation, especially when the strain range under consideration is within the linear region.

Due to the anisotropic nature of the rectal wall, in this paper the stress-strain relation will be discussed in context of orthotropic model. The principal directions of the material are along the x_1-, x_2-, and x_3-axes, and thus there are totally nine independent material parameters to be determined (see Appendix A for details). The tangential moduli are estimated through the strain offset method in the range of 0.4–0.6 using a linear regression algorithm. As such, the effective tangents are approximately determined with an average regression constant R^2 equal to 0.98. The effective tensile resistances along the longitudinal axis, E_1, and along the transverse axis, E_2, are determined through the tensile stress-strain curves along the x_1- and x_2-directions, respectively. The effective out-of-plane compression resistance, E_3, is calculated using the compression curves along the x_3-direction. Through the shear experiments with the shear plane normal to the x_3 axis and the shear directions along the x_1 and x_2 axes, the effective shear resistances, G_{13} and G_{23}, can be obtained.

The tensile tests along the inclined direction, x_{inc}, provide comprehensive information of the effective in-plane Poisson's ratio, ν_{12}, and in-plane shear resistance G_{12}. The effective tensile resistance along x_{inc}, E_{n}, is related to E_1 and E_2 through (see Appendix A)

$$E_n = \frac{n^4}{E_1} + \left(\frac{1}{G_{12}} - 2\frac{\nu_{12}}{E_1}\right)m^2n^2 + \frac{m^4}{E_2} \qquad (4)$$

Hence, with the value of ν_{12} obtained through the self-correlation image analysis of the high resolution photos taken in the tensile tests, G_{12} can be calculated using the parameters obtained above. Finally, The remaining two out-of-plane effective Poisson's ratios (ν_{13} and ν_{23}) were estimated by optimizing the constraints on the symmetry of the tangential stiffness matrix and positive strain energy [25, 26], and the results are listed in Table I. The standard deviations are estimated based on the calibration data.

TABLE I The tangential moduli and effective Poisson's ratios of the rectal wall

Properties	Mean value	Standard derivation
E_1 (kPa)	59.9	8.6
E_2 (kPa)	147.0	20.6
E_3 (kPa)	37.3	5.7
G_{12} (kPa)	29.3	—
G_{13} (kPa)	10.7	6.9
G_{23} (kPa)	40.6	9.6
ν_{12}	0.54	0.12
ν_{13}	0.32	—
ν_{23}	0.59	—

According to Table I and the stress-strain curves shown in Fig. 3, it can be seen that at the early stage the tensile resistance of the rectal wall is quite low, while if the effective strain exceeds a critical value, ε_{cr}, the tangential modulus become much larger. The critical strain is of the maximum value around 40% along the longitudinal direction and the minimum value around 13% along the transverse direction. Along the inclined direction, $\varepsilon_{\text{cr}} \approx 33\%$ is somewhat in between. Furthermore, it is noticed that the effective tensile resistance along the axial direction, E_1, is much smaller than that along the circumferential direction, E_2, which is in consistent with the fact that the number density of fibers along the x_2 axis is higher than that along the x_1 axis.

These phenomena should be attributed to the sigmoidal structure of the rectal wall consisting of a large number of horizontal folds with the characteristic width ranging from sub-μm level to sub-mm level [8]. During the tensile experiment along direction x_1, since the tensile resistance of the large folds is lower than that of small folds, the larger ones will be unfolded first, resulting in the low beginning tensile resistance discussed above. At ε_{cr}, most of the large folds have been unfolded and more and more small ones are involved in the load bearing sections, and as a result the tangential modulus becomes increasingly high. Eventually when all the folds are unfolded the testing curve should reflect the intrinsic response of tissue fibrils. At this stage the effective modulus can be much higher than E_1 and the strain is around 300–500% [27], which is beyond the range of the microtesting system and is of little interest for clinical practices.

Along the transverse direction, on the other hand, the number and the size of longitudinal folds are much lower than that of the horizontal ones, except for the end area of the rectum. Therefore, the critical strain at which the large folds are unfolded is much lower than that along the x_1 axis and, also due to the relatively high number density of fibers, the tensile resistance is much higher. Note that the effective out-of-plane shear modulus G_{23} is larger than G_{13}, which agrees with the trend of the effective tensile moduli.

Fig. 4 shows the out-of-plane compression resistance curve. Through Table I, it can be seen that E_3 is smaller than both of E_1 and E_2. Although the compression resistance and the tensile resistance are not necessarily the same, this result demonstrates clearly that the rectal wall is more compliant under the out-of-plane loading than under the in-plane loading, which should be related to the layered structure consisting of the soft matrix. We also remark that after the compressive strain exceeds the proportional limit, E_3 decreases as the strain rises, resembling the behavior of a foamed material [28]. One the other hand, the high values of the effective Poisson's ratios around 0.5 suggest that the rectal wall is incompressible. A deeper understanding of these phenomena must be based on examining the details of the microstructure of soft tissues.

Clearly, the calculation of the tangential moduli discussed above gives only a first-order description of the mechanical properties and does not constitute a fully developed model. In order to accurately simulate the mechanical behavior of rectal walls, hyperelastic or viscoelastic theories must be considered.

Conclusions

By using a two-compound-flexure microtesting system, the applied load and deformation of specimens of rectal wall can be measured accurately. The experimental data reveal that the rectal wall is orthotropic. At relatively small strain, the tensile resistance along all the directions is quite low, and when the strain exceeds a critical value significant effective strain hardening occurs. The following conclusions are drawn:

(1) The tangential moduli along different directions, E_1, E_2, and E_3, differ from each other significantly.

(2) The tensile resistance along the longitudinal direction is much lower than that along the transverse direction, which can be attributed to the high number density of horizontal folds in the rectal wall.

(3) The compliance of the rectal wall under out-of-plane loading is higher than that under in-plane loading.

(4) Due to the pronounced nonlinear and time-dependent characteristics, in order to study the mechanical behavior of the rectal wall in a broad strain range, hyperelastic and/or viscoelastic theories must be employed.

Appendix A

The material Cartesian coordinate system (x_1, x_2, x_3) of the rectal wall is shown in Fig. 1. The (x_1, x_2)-plane is within the rectal wall and the x_3-axis is along the out-of-plane direction. In the rectal wall, the x_1-axis is along the longitudinal direction while the x_2-axis is along the transverse direction. Assuming that in the linear region of the response curve the rectal wall is orthotropic, we then have the following constitutive relationship between the strain (normal and shear) and stress (normal and shear):

$$\begin{pmatrix} \varepsilon_1 \\ \varepsilon_2 \\ \varepsilon_3 \\ \gamma_{23} \\ \gamma_{13} \\ \gamma_{12} \end{pmatrix} = \left(A_{ij}\right) \begin{pmatrix} \sigma_1 \\ \sigma_2 \\ \sigma_3 \\ \tau_{23} \\ \tau_{13} \\ \tau_{12} \end{pmatrix} \tag{A1}$$

where (A_{ij}) is the compliance matrix of the material, which for the orthotropic case can be expressed as

$$(A_{ij}) = \begin{pmatrix} \frac{1}{E_1} & -\frac{\nu_{21}}{E_2} & -\frac{\nu_{31}}{E_3} & 0 & 0 & 0 \\ -\frac{\nu_{12}}{E_1} & \frac{1}{E_2} & -\frac{\nu_{32}}{E_3} & 0 & 0 & 0 \\ -\frac{\nu_{13}}{E_1} & -\frac{\nu_{23}}{E_2} & \frac{1}{E_3} & 0 & 0 & 0 \\ 0 & 0 & 0 & \frac{1}{G_{23}} & 0 & 0 \\ 0 & 0 & 0 & 0 & \frac{1}{G_{13}} & 0 \\ 0 & 0 & 0 & 0 & 0 & \frac{1}{G_{12}} \end{pmatrix} \quad i, j = 1, 2, \ldots, 6 \tag{A2}$$

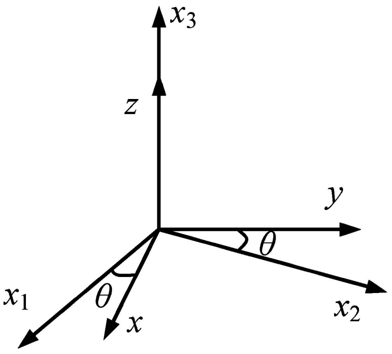

Figure A1 Relationship between two Cartesian coordinate systems (x, y, z) and (x_1, x_2, x_3), with the latter being rotated by an angle of θ from the material coordinate system in the (x_1, x_2)-plane.

We now introduce a new Cartesian coordinate system (x, y, z) which is rotated by θ in the (x_1, x_2)-plane with respect to the material coordinate system (see Fig. A1). In the new system, the constitutive relation becomes

$$\begin{pmatrix} \varepsilon_x \\ \varepsilon_y \\ \varepsilon_z \\ \gamma_{yz} \\ \gamma_{xz} \\ \gamma_{xy} \end{pmatrix} = (a_{ij}) \begin{pmatrix} \sigma_x \\ \sigma_y \\ \sigma_z \\ \tau_{yz} \\ \tau_{xz} \\ \tau_{xy} \end{pmatrix} \tag{A3}$$

where the new compliance matrix (a_{ij}) is of the following non-zero elements

$$\begin{aligned}
a_{11} &= \frac{n^4}{E_1} + \left(\frac{1}{G_{12}} - 2\frac{\nu_{12}}{E_1}\right)m^2n^2 + \frac{m^4}{E_2}; \\
a_{22} &= \frac{m^4}{E_1} + \left(\frac{1}{G_{12}} - 2\frac{\nu_{12}}{E_1}\right)m^2n^2 + \frac{n^4}{E_2} \\
a_{12} &= \left(\frac{1}{E_1} + \frac{1}{E_2} + 2\frac{\nu_{12}}{E_1} - \frac{1}{G_{12}}\right)m^2n^2 - \frac{\nu_{12}}{E_1}; \\
a_{16} &= \left[2\frac{m^2}{E_2} - 2\frac{n^2}{E_1} + \left(\frac{1}{G_{12}} - 2\frac{\nu_{12}}{E_1}\right)(n^2 - m^2)\right]mn \\
a_{26} &= \left[2\frac{n^2}{E_2} - 2\frac{m^2}{E_1} - \left(\frac{1}{G_{12}} - 2\frac{\nu_{12}}{E_1}\right)(n^2 - m^2)\right]mn; \\
a_{66} &= 4\left(\frac{1}{E_1} + \frac{1}{E_2} + 2\frac{\nu_{12}}{E_1} - \frac{1}{G_{12}}\right)m^2n^2 + \frac{1}{G_{12}} \\
a_{13} &= -\frac{\nu_{23}}{E_2}m^2 - \frac{\nu_{13}}{E_1}n^2 = -\frac{\nu_{23}}{E_2}m^2 - \frac{\nu_{31}}{E_3}n^2; \\
a_{23} &= -\frac{\nu_{23}}{E_2}n^2 - \frac{\nu_{13}}{E_1}m^2 = -\frac{\nu_{23}}{E_2}n^2 - \frac{\nu_{31}}{E_3}m^2 \\
a_{33} &= \frac{1}{E_3}; \; a_{36} = 2\left(\frac{\nu_{13}}{E_1} - \frac{\nu_{23}}{E_2}\right)mn \\
&= 2\left(\frac{\nu_{31}}{E_3} - \frac{\nu_{23}}{E_2}\right)mn; \; a_{44} = \frac{n^2}{G_{23}} + \frac{m^2}{G_{13}} \\
a_{45} &= \left(\frac{1}{G_{23}} - \frac{1}{G_{13}}\right)mn; a_{55} = \frac{m^2}{G_{23}} + \frac{n^2}{G_{13}}
\end{aligned} \tag{A4}$$

where $m = \sin\theta$ and $n = \cos\theta$.

Acknowledgment

We are grateful to Dr. D. Yan in the William Beaumont Hospital for the useful discussions. Special thanks are also due to the reviewer of this paper who provided insightful suggestions. This work is partly sponsored by NCI grant R01CA091020 (JL).

References

1. J. LIANG and D. YAN, *Med. Phys.* **30** (2003) 2116.
2. D. YAN, D. A. JAFFRAY and J. W. WONG, *Int. J. Radit. Oncol.* **44** (1999) 665.
3. K. K. BROCK, D. L. MCSHAN, R. K. T. HAKEN, S. J. HOLLISTER, L. A. DAWSON and J. M. BALTER, *Med. Phys.* **30** (2003) 290.
4. A. BOUNAIM, S. HOLM, W. CHEN, A. ODEGARD, A. TVEITO and K. THOMENIUS, *Lect. Notes Comput. Sci.* **2668** (2003) 705.
5. D. LI, P. M. MEANEY and K. D. PAULSEN, *IEEE T. Microw. Theory* **51** (2003) 1179.
6. G. SREENIVASA, J. GELLERMANN, B. RAU, J. NADOBNY, P. SCHLAG, P. DEUFLHARD, R. FELIX and P. WUST, *Int. J. Radiat. Oncol.* **55** (2003) 407.
7. T. G. BECKWITH, R. D. MARANGONI and J. H. LIENHARD, in "Mechanical Measurements" (Addison Wesley, Reading MA, 1993) p. 45.
8. Y. C. FUNG, in "Biomechanics: Mechanical Properties of Living Tissues" (Springer, NY, 1993).
9. K. KROGH, A. M. RYHAMMER, L. LUNDBY, H. GREGERSEN and S. LAURBERG, *Dis. Colon Rectum* **44** (2001) 196.
10. O. H. GILJA, A. HEIMDAL, T. HAUSKEN, H. GREGERSEN, K. MATRE, A. BERSTAD and S. ODEGAARD, *Ultrasound Med. Biol.* **28** (2002) 1457.
11. H. GREGERSEN, J. BARLOW and D. THOMPSON, *Neurogastroent Motil.* **11** (1999) 109.
12. R. J. F. FELT-BERSMA, C. E. J. SLOOTS, A. C. POEN, M. A. CUESTA and S. G. M. MEUWISSEN, *Dis. Colon Rectum* **43** (2000) 1732.
13. R. SCHAFER, NB. SCHUMACHER, S. KLOSTERHALFEN and P. ENCK, *Gastrpenterology* **108** (1995) A684.
14. M. NAGASHIMA, N. IWAI, J. YANAGIHARA and G. IWATA, *Eur. J. Pediatr. Surg.* **5** (1995) 167.
15. G. N. RAO, P. J. DREW, J. R. T. MONSON and G. S. DUTHIE, *Int. J. Colorectal. Dis.* **12** (1997) 33.
16. F. H. DALL, C. S. JORGENSEN, D. HOUE, H. GREGERSEN and J. C. DJURHUUS, *Gut* **34** (1993) 1581.
17. J. C. BARON, P. ARHAN, L. BOCCONGIBOD and L. BOCCONGIBOD, *Urol. Res.* **20** (1992) 247.
18. M. FU and J. Z. ZHANG, *J. Pediatr. Surg.* **32** (1997) 7.
19. B. D. JENSEN, M. P. DE BOER, N. D. MASTERS, F. BITSIE and D. A. LA VAN, *J. MEMS* **10** (2001) 336.
20. S. GREEK, F. ERICSON, S. HOHANSSON, M. FURTSCH and A. RUMP, *J. Micromech. Microeng.* **9** (1999) 245.
21. H. D. ESPINOSA, B. C. PROROK and M. FISCHER, *J. Mech. Phys. Solids* **51** (2003) 47.
22. W. N. SHARPE, K. M. JACKSON, K. J. HEMKER and Z. XIE, *J. Micromech. Microeng.* **3** (1997) 317.
23. D. T. Read, *Mech. Mater.* **6** (1998) 11.
24. S. GUDLAVALLETI and L. ANAND, in Proceedings of the 2001 ASME IMECE (New York, November 2001).
25. P. M. THOMPSON and A. W. TOGA, *Comput. Visual Sci.* **5** (2002) 13.
26. T. BELYTSCHKO, W. K. LIU and B. MORAN, in "Non-linear Finite Elements for Continua and Structure" (John Wiley & Sons, 2003).
27. F. A. DUCK, in "Physical Properties of Tissue: A Comprehensive Reference Book" (Academic Press, 1990).
28. J. BANHART, *Prog. Mater. Sci.* **46** (2001) 559.

Received 20 February
and accepted 19 February 2004